Published in final edited form as:
Neuroimage. 2012 October 15; 63(1): 194–202. doi:10.1016/j.neuroimage.2012.06.048.

Hippocampal CA1 apical neuropil atrophy and memory performance in Alzheimer's disease

Geoffrey A. Kerchner[a,*], **Gayle K. Deutsch**[a], **Michael Zeineh**[b], **Robert F. Dougherty**[c], **Manojkumar Saranathan**[b], and **Brian K. Rutt**[b]

[a]Stanford Center for Memory Disorders, Department of Neurology and Neurological Sciences, Stanford University School of Medicine, Stanford, CA 94305, USA

[b]Department of Radiology, Stanford University School of Medicine, Stanford, CA 94305, USA

[c]Stanford Center for Neurobiological Imaging, Department of Psychology, Stanford University, Stanford, CA 94305, USA

Abstract

Memory loss is often the first and most prominent symptom of Alzheimer's disease (AD), coinciding with the spread of neurofibrillary pathology from the entorhinal cortex (ERC) to the hippocampus. The apical dendrites of hippocampal CA1 pyramidal neurons, in the stratum radiatum/stratum lacunosum-moleculare (SRLM), are among the earliest targets of this pathology, and atrophy of the CA1-SRLM is apparent in postmortem tissue from patients with mild AD. We previously demonstrated that CA1-SRLM thinning is also apparent in vivo, using ultra-high field 7-Tesla (7 T) MRI to obtain high-resolution hippocampal microstructural imaging. Here, we hypothesized that CA1-SRLM thickness would correlate with episodic memory performance among patients with mild AD. We scanned nine patients, using an oblique coronal T2-weighted sequence through the hippocampal body with an in-plane resolution of 220 μm, allowing direct visual identification of subfields — dentate gyrus (DG)/CA3, CA2, CA1, and ERC — and hippocampal strata — SRLM and stratum pyramidale (SP). We present a novel semi-automated method of measuring stratal width that correlated well with manual measurements. We performed multi-domain neuropsychological evaluations that included three tests of episodic memory, yielding composite scores for immediate recall, delayed recall, and delayed recognition memory. Strong correlations occurred between delayed recall performance and the widths of CA1-SRLM (r^2=0.69; p=0.005), CA1-SP (r^2=0.5; p=0.034), and ERC (r^2=0.62; p=0.012). The correlation between CA1-SRLM width and delayed recall lateralized to the left hemisphere. DG/CA3 size did not correlate significantly with any aspect of memory performance. These findings highlight a role for 7 T hippocampal microstructural imaging in revealing focal structural pathology that correlates with the central cognitive feature of AD.

Keywords

Alzheimer's disease; Dementia; Hippocampus; CA1; Memory; Neuropsychology; Magnetic resonance imaging; Structural imaging

[*]Corresponding author at: Department of Neurology and Neurological Sciences, Stanford University School of Medicine, 300 Pasteur Drive, Room A343, MC5235, Stanford, CA 94305-5235, USA. Fax: +1 650 723 7434. kerchner@stanford.edu (G.A. Kerchner).

Introduction

Episodic memory dysfunction is the earliest and most profound symptom in most cases of Alzheimer's disease (AD). The hippocampus plays a key role in the consolidation of new episodic memories (Milner, 2005), and neuropathological alterations of this structure (Braak et al., 2006) probably account for early symptoms of the disease.

Hippocampal degeneration in early AD is not uniform. After inundation of the entorhinal cortex (ERC) by neurofibrillary tangle pathology, the synapse-rich CA1 stratum radiatum and stratum lacunosummoleculare (SRLM) is the next area to become affected (Braak and Braak, 1997; Braak et al., 2006; Thal et al., 2000). The appearance of aggregates of the microtubule-associated protein tau in CA1-SRLM precedes the loss of CA1 pyramidal neurons themselves, and coincides with the earliest cognitive symptoms (Braak and Braak, 1997; Thal et al., 2000). At autopsy, profound synaptic loss and atrophy appears in this area (Braak and Braak, 1997; Mizutani and Kasahara, 1997; Qin et al., 2004; Scheff et al., 2007; Thal et al., 2000).

Confirming the predictions of this postmortem literature, CA1-SRLM atrophy distinguished patients with mild AD from age-matched normal controls (Kerchner et al., 2010). This prior study took advantage of the ability of ultra-high field 7-Tesla (7 T) magnetic resonance imaging (MRI) to reveal distinct hippocampal subfield and stratal boundaries, including a separation between CA1-SRLM and the adjacent cell body layer, the stratum pyramidale (CA1-SP) (Kerchner, 2011; Kerchner et al., 2010). Using lower field imaging techniques not designed to discriminate between hippocampal strata, other labs have observed general volume loss in CA1 or adjacent subiculum in conjunction with normal aging (La Joie et al., 2010), Mild Cognitive Impairment (MCI) (Apostolova et al., 2006a; Mueller et al., 2010; Yassa et al., 2010), and AD (Apostolova et al., 2006a; Mueller et al., 2007, 2010). One group has shown that CA1 atrophy predicts future cognitive decline among healthy subjects (Apostolova et al., 2010b) or patients with MCI (Apostolova et al., 2006b). In our prior study, CA1-SP thickness did not differ between subjects with mild AD or normal cognition (Kerchner et al., 2010), suggesting that CA1-SRLM atrophy could conceivably be driving the findings of other groups. Only one group found atrophy in the dentate gyrus (DG) and CA3 to be greater than in CA1 among patients with MCI (Yassa et al., 2010).

There is likely a connection between early episodic memory dysfunction and early CA1 neurofibrillary pathology in AD. Indeed, others have reported correlations between overall CA1 size and delayed memory performance (Apostolova et al., 2010a; Atienza et al., 2011;Mueller et al., 2011a), and other work suggests a specific role for CA1 in the recollection of recently learned cues (Eldridge et al., 2005). Given the special vulnerability of the CA1 apical neuropil to early AD, we hypothesized that CA1-SRLM thickness should correlate with delayed recall performance among patients. Using a new T2-weighted 7 T MRI sequence for microstructural imaging of the medial temporal lobe, together with a novel method of stratal width determination, we endeavored to test this hypothesis in patients with mild AD.

Methods

Subjects

Patients with mild AD were recruited from the Stanford Center for Memory Disorders. Each subject provided written, informed consent in accordance with a protocol approved by the Stanford Institutional Review Board. Inclusion criteria included a diagnosis of probable AD (amnestic presentation) according to the National Institute on Aging-Alzheimer's Association criteria (McKhann et al., 2011), a Clinical Dementia Rating (CDR) score of 0.5

or 1 (Morris, 1993), and sufficient English language skills to participate in the neuropsychological assessment. Exclusion criteria included any contraindication to MRI, a history of stroke or other structural brain abnormality, or the presence of any neurological or medical condition other than AD that could interfere with normal cognition. One subject was excluded after enrolling because of technical problems with the MRI scan. Subject characteristics appear in Table 1. All subjects were right-handed.

Clinical assessment

Each subject underwent a clinical evaluation that included a history, physical examination, and neurological examination by a physician at the Stanford Center for Memory Disorders. The faculty of the Center, including neurologists and neuropsychologists, discussed each potential subject in a consensus conference to determine a research diagnosis. With an identified study partner (usually a spouse), each recruited subject then underwent a functional assessment that included the CDR (Morris, 1993), Neuropsychiatric Inventory (Cummings et al., 1994), the Geriatric Depression Scale (Yesavage, 1988), and the Functional Assessment Questionnaire (Pfeffer et al., 1982). The main study metrics included a neuropsychological battery and a 7 T MRI scan, as described below. For each subject, all study metrics were acquired within an average window of 36 days (range 2–132).

Neuropsychological assessment

Psychometric tests were administered by a trained psychometrician who was blinded to the imaging data and who was not involved in any other aspect of the study.

Memory was assessed using the Hopkins Verbal Learning Test-Revised (HVLT-R) (Brandt, 1991), the Brief Visuospatial Memory Test-Revised (BVMT-R) (Benedict, 1997), and the Logical Memory (LM) subtest of the Wechsler Memory Scale, 3rd edition (WMS-III) (Wechsler, 1997). We derived metrics of immediate recall, delayed recall, and delayed recognition from each test as follows: Immediate recall on the HVLT-R or BVMT-R was the sum correct responses on the three learning trials; on the LM test, it was the Logical Memory 1 score. Delayed recall on the HVLT-R or BVMT-R was the number of correct responses on the delayed free recall trial; on the LM test, it was the Logical Memory 2 score. Delayed recognition on the HVLT-R or BVMT-R was the discrimination index, or sum of hits minus false positives on the recognition trial; on the LM test, it was the total correct responses on the recognition subtest. Composite immediate recall, delayed recall, and delayed recognition metrics were obtained by rescaling raw scores from 0 (set at the minimum score for the group) to 1 (the maximum score) and averaging across tests.

The battery of neuropsychological tests also included, for language, the Boston Naming Test; for visuospatial function, the figure copy subtest of the Repeatable Battery for the Assessment of Neuropsychological Status (RBANS) (Randolph et al., 1998), and the Block Design and Matrix Reasoning subtests of the Wechsler Abbreviated Scale of Intelligence (WASI) (Wechsler, 1999); for working memory, the digit span subtest of the WMS-III; and for executive function, Category Fluency (Gladsjo et al., 1999) and Trail-Making Test. Raw scores from these tests were used for analysis.

Image acquisition

Subjects were scanned on a 7 T GE Signa HDx whole-body MRI scanner (GE Healthcare, General Electric Company, Waukesha, WI) using a 16-channel radiofrequency receive head coil contained within a quadrature transmit coil (Nova Medical, Inc., Wilmington, MA). The subject's head was stabilized by packing foam between the temples and the inner surface of the receive coil to minimize motion during the scan, and a plethysmograph was placed on a finger on the right hand to monitor peripheral pulse. Imaging was targeted to the medial

temporal lobes, with acquisition of oblique coronal images oriented perpendicular to the longitudinal axis of the hippocampus, using a T2-weighted fast spin echo (FSE) sequence: effective echo time (TE) 49 ms; repetition time (TR) ~5–6 s (cardiac gated, with the R-R interval set for each subject according to their average heart rate, so as to achieve a TR within this range); nominal excitation flip angle 90°; tailored refocusing flip angle from 160° to 130°; echo train length (ETL) 8; bandwidth 20.8 kHz; number of excitations (NEX) 1; slice thickness 1.5 mm; slice gap 0.5 mm; field-of-view 170×170 mm^2; acquisition matrix 768×768, yielding acquired voxels measuring 0.22×0.22×1.5 mm^3. Images were interpolated on the scanner by zero filling k-space to a 1024×1024 matrix yielding a reconstructed voxel size of 0.166×0.166×1.5 mm^3. Specific absorption rate (SAR) was approximately 2.5 W/kg. Typically 16–18 slices were obtained per subject covering most or all of the head of the hippocampus, the entire body, and some of the tail (Fig. 1). Scan time was typically just less than 10 min.

Image analysis

Images were visualized with the OsiriX 3.9 software package (Rosset et al., 2004) (http://www.osirix-viewer.com/) and with FSL-View, a component of the FSL 4.1 software package (http://www.fmrib.ox.ac.uk/fsl/). Selection of slices and delineation of regions of interest were performed by a single scientist (GK) according to the following procedures:

Landmarks

Because the landmarks allowing visual identification of hippocampal subfields are most apparent in the hippocampal body (Kerchner et al., 2010) (Fig. 1), slices through the hippocampal body were chosen for analysis of subfield dimensions. From anterior to posterior, the hippocampal body was delimited from the first slice in which the uncus was not present (Fig. 1G) to the level of the colliculi (Fig. 1N). Although hippocampal subfields are defined not by their imaging characteristics but rather by cytoarchitecture (and we did not have histological specimens for any of the subjects in this study), the subfield boundaries described here could be consistently observed in all scans and occurred in expected locations based on human hippocampal atlases (Amaral and Lavenex, 2007; Insausti and Amaral, 2012; Prudent et al., 2010; Yushkevich et al., 2009). The dentate gyrus (DG) and CA3 subfields were not separable at this resolution (Kerchner et al., 2010), and so these subfields were analyzed together. The medial boundary of the CA2 subfield was identified where the SP emerged out of CA3 and reached its narrowest thickness, and its lateral boundary was where SP began to widen (Fig. 1Q). A CA1/CA2 transition zone appeared on most slices where SP gradually widened to its full thickness (Fig. 1Q), and CA1 was defined as starting from that point and ending near the medial border of DG. The boundary between CA1 and subiculum overlaps histologically, with the subiculum characterized by a lower density and more layered arrangement of neurons than CA1 (Insausti and Amaral, 2012), likely corresponding to a reduction in T2 signal intensity within the SP at the medial extent of CA1 (Fig. 1). This transition zone migrated medially on more posterior slices (Figs. 1A–P), as would be expected based on histological observations (Insausti and Amaral, 2012). We measured CA1-SP, CA1-SRLM, and ERC thicknesses; and DG/CA3 and hippocampal cross-sectional areas.

DG/CA3

The DG/CA3 was measured by outlining its circumference using OsiriX and computing the cross-sectional area on each slice. Values were averaged across slices to yield one value per side per subject.

CA1 stratal width determination

We developed a semi-automated method for measuring the thickness of CA1-SP and CA1-SRLM. The CA1-SRLM was defined as the hypointense band between CA1-SP and the DG, which were relatively hyperintense (Fig. 1Q) (Kerchner et al., 2010). The hippocampal sulcus, usually vestigial, intervenes in this space; any area containing a visible pocket of CSF (T2 intensity similar to the ventricles) was excluded from the following routine:

The region of interest (CA1-SP or CA1-SRLM) was specified by drawing a line through its middle (Fig. 2A) on each slice through the hippocampal body, using FSL-View. MATLAB (MathWorks, Inc., Natick, MA) was used to fit a spline to this user-specified line, and then to derive orthogonal vectors along this spline (Fig. 2A). T2 signal intensity was plotted along each vector as a function of distance from the spline. To mitigate any bias from the tendency of the user-specified line to lie more to one side or the other of the true midpoint of the structure of interest, each signal intensity-distance function was averaged with its corresponding reverse function, yielding symmetric arrays. All such arrays on a slice were then averaged together, and a spline was fit to the result, yielding a curve with a trough at distance zero in the case of CA1-SRLM (Fig. 2B), or a peak in the case of CA1-SP. The first derivative of this curve was calculated, and the distance from the peak to the trough of this first derivative (corresponding to the inflection points on the original curve) was taken as the width of the corresponding region (Fig. 2B). The left and right hippocampi were analyzed separately, and values from each slice were averaged to yield one value per side per subject.

CA1-SP and CA1-SRLM widths were also measured manually, following the previously published method (Kerchner et al., 2010): In OsiriX, three thickness measurements were made along the length of each structure on each of the same slices used for the semi-automated method; thickness was defined as the distance from one tissue interface to another using an orthogonal line. These values were averaged to yield one value per side per subject.

Hippocampus

In addition to these subfield measurements, mean hippocampal cross-sectional area was calculated by manually tracing the circumference of the hippocampus on each slice through the hippocampal body using OsiriX. The medial boundary of the hippocampus was defined as the medial border of DG. Values were averaged across slices to yield one value per side per subject.

Entorhinal cortex

The ERC was identified on slices starting with the most anterior slice in which the alveus was visible (Fig. 1A) to the most posterior slice on which the uncus appeared (Fig. 1F). This captured only a posterior part of the ERC, which actually extends rostrally toward the temporal pole, but this anterior portion was outside the field of view of most subjects. The method that we describe allowed a standardized approach across our subjects. Within a slice, the superomedial edge of the ERC was defined as the upper medial corner of the parahippocampal gyrus, where it was noted that cortical signal intensity increased and became uniform (Fig. 1R). The inferolateral edge was defined as the medial base of the collateral sulcus, where the basal edge of the cortex reached a point of maximum curvature; while the ERC probably extends further into the sulcus than this, no border could be visualized between ERC and perirhinal cortex. OsiriX was used to outline the perimeter of the ERC (e.g., the curved trapezoid enclosed by the dotted and solid lines in Fig. 1R) and to measure the lengths of the two edges (the dotted lines in Fig. 1R); thickness was approximated as:

$$2 \times \frac{(\text{trapezoid area})}{(\text{trapezoid circumference}) - (\text{sum of the lengths of the edges})}.$$

Other considerations

We used raw metrics for the following reasons: We previously found that normalization to total intracranial volume did not influence data interpretation (Kerchner et al., 2010); the imaging technique in this study did not include whole brain coverage and did not provide an estimate of intracranial volume; and laminar dimensions of the hippocampus and cortex are likely driven by the absolute dimensions of neurons and their neurites and by presence of pathology, rather than by arbitrary intersubject differences in head size. We did not measure CA2-SP or CA2-SRLM thickness, because CA2 was typically quite short (Fig. 1Q) and in many subjects was not amenable to the semi-automated routine described above. The *stratum oriens* (i.e., basal neuropil, or the hypointense band peripheral to the SP) was too thin to measure reliably and was indistinguishable from the alveus. Although we could have measured volumes rather than thicknesses or areas, the third (longitudinal) dimension would have been a quantal metric reflecting only the number of slices analyzed, and would have added unnecessary noise and no additional information into our calculations.

Statistics

Data are reported as means ± standard deviations. For correlational analyses, the Pearson coefficients were calculated, and two-tailed p values were used to test for significance. A trend was defined as $p<0.1$, and the threshold for significance was $p<0.05$. For comparisons between correlation coefficients, Steiger's Z statistic was calculated (Meng et al., 1992), and two-tailed p values were used.

Results

Validation of semi-automated stratal width measurements

We measured CA1-SP and CA1-SRLM widths using both manual and semi-automated techniques (see Methods). The values correlated significantly (for CA1-SP, $r=0.74$, $p<0.001$; for CA1-SRLM, $r=0.75$, $p<0.001$). Unless otherwise stated, semi-automated measurements were used below.

Relationship of medial temporal microstructure with memory performance

We tested whether medial temporal microstructural metrics correlated with immediate recall, delayed recall, or delayed recognition memory (Fig. 3 and Table 2). For immediate recall, there was no significant relationship with any microstructural measurement. By contrast, delayed recall did correlate significantly with the widths of CA1-SRLM, CA1-SP, and ERC. For delayed recognition, significant correlations emerged with CA1-SRLMand ERC widths. These patterns of significance were the same whether CA1-SRLM and CA1-SP thicknesses were measured with manual or semi-automated techniques (Table 2). DG/CA3 cross-sectional area did not correlate significantly with any aspect of memory performance. Mean hippocampal cross-sectional area, a proxy for total hippocampal volume (see Section Hippocampus), correlated with delayed recall but not with delayed recognition or immediate recall (Table 2).

In the correlational tests described above, imaging metrics were averaged for the left and right sides, yielding, for instance, one value for CA1-SRLM per subject. Upon examining the sides individually, we found that CA1-SRLM width correlated with delayed recall better on the left than right ($p<0.05$ using Steiger's Z statistic) (Meng et al., 1992). Such

comparisons were not significant for other composite memory scores or structural metrics. Out of a concern that left and right hippocampi contribute differentially to verbal and visuospatial memory (Frisk and Milner, 1990; Milner, 1965; Nunn et al., 1998, 1999; Petrides and Milner, 1982; Smith and Milner, 1981; Spiers et al., 2001), we tested correlations between microstructural metrics from each hemisphere independently and scores from each individual memory test (Table 3). We found that for LM, a test of verbal contextual memory, delayed recall correlated with CA1-SRLM width better on the left ($p<0.01$ by Steiger's Z; Table 3), and delayed recognition correlated with ERC width better on the left ($p<0.05$). Such direct comparisons for the HVLT-R and BVMT-R were not significant, although we noted a tendency, especially on comparisons between CA1-SRLM width and BVMT-R performance, for left- but not right-sided correlation coefficients to achieve statistical significance (Table 3).

By contrast, hippocampal metrics were symmetric, on average, among our subjects: No lateralized size differential was observed ($p>0.05$ by two-tailed paired t-test) for CA1-SRLM (left 0.54 ± 0.09 mm; right 0.52 ± 0.07 mm; using semi-automated data), CA1-SP (left 1.3 ± 0.2 mm; right 1.4 ± 0.2 mm; using semi-automated data), DG/CA3 (left 11 ± 2 mm^2; right 11 ± 2 mm^2), or mean hippocampal cross-sectional area (left 41 ± 10 mm^2; right 40 ± 8 mm^2). ERC was thinner on the left (left 1.9 ± 0.2 mm; right 2.1 ± 0.2 mm; $p=0.021$). Hippocampal cross-sectional area was tightly matched across the hemispheres among subjects ($r^2=0.8$; $p=0.001$). On the other hand, subfield metrics did appear to vary independently from side to side between subjects, with no significant interhemispheric correlations among subjects for CA1-SRLM width ($r^2=0.29$; $p=0.13$; using semi-automated data), CA1-SP width ($r^2=0.13$; $p=0.34$; using semi-automated data), or DG/CA3 area ($r^2=0.41$; $p=0.065$). Left and right ERC widths did correlate significantly ($r^2=0.45$; $p=0.049$).

Relationship of medial temporal microstructure with other neuropsychological traits

We next tested whether the same microstructural metrics correlated with performance on neuropsychological tests that are thought to be hippocampal-independent (Table 2). Not surprisingly, there were very few direct correlations on tests of working memory, confrontational naming, visuospatial ability, or executive function. Manually-derived measures of CA1-SRLM thickness correlated negatively with digit span and positively with figure copy. DG/CA3 cross-sectional area correlated positively with full scale IQ. No other significant correlations emerged. Medial temporal microstructural metrics did not correlate with age, years of education, or gender (Table 2).

One possible explanation for absent correlations could be that test scores were highly skewed, as could occur if many subjects performed badly. However, we observed a good spread in performance on most tests, and the ratio of skewness to the standard error of skewness was in the acceptable range of −2 to 2 (mean 0.46, with zero indicating no skew) for each neuropsychological test administered, including the tests of memory; the one exception was the Trails B test, for which the ratio was −2.3.

Relationships between medial temporal microstructural metrics

Given that different areas of the medial temporal lobe are differentially affected by pathology in AD (Braak and Braak, 1997; Braak et al., 2006), and that corresponding microstructural imaging metrics are variously sensitive for AD (Kerchner et al., 2010), we tested how well the dimensions of individual subfield correlated with each other (Table 2). CA1-SP and ERC widths were tightly correlated. Not surprisingly, there were also significant correlations between subfield metrics and mean hippocampal cross-sectional area.

Discussion

Our findings support the hypothesis that CA1-SRLM thickness correlates with delayed recall memory performance among patients with mild AD. We additionally found that the thicknesses of CA1-SP and ERC similarly correlated with delayed recall. These data establish that in addition to a role in discriminating patients with AD from healthy controls (Kerchner et al., 2010), hippocampal microstructural metrics also track the severity of a core neuropsychological feature of the disease.

CA1-SRLM atrophy and memory dysfunction

Our study is the first to consider the differential associations of CA1-SP and CA1-SRLM atrophy with delayed recall performance in vivo. Distinguishing the principal neuronal cell body layer from its associated apical neuropil was possible because of the remarkably high resolution and signal-to-noise afforded by 7 T MRI (Kerchner, 2011; Kerchner et al., 2010). Attention to this layered anatomy is relevant, because disproportionate CA1-SRLM thinning is an early manifestation of AD that has been observed at autopsy (Braak and Braak, 1997; Mizutani and Kasahara, 1997; Qin et al., 2004; Scheff et al., 2007; Thal et al., 2000) and by 7 T MRI in vivo (Kerchner et al., 2010).

CA1-SRLM atrophy could play a mechanistic role in the memory loss associated with AD. It is an area rich in synapses from CA3 to CA1 and from perforant pathway axons from the ERC to CA1. Synapses onto CA1 neurons, especially in the stratum radiatum, are highly plastic and have been hypothesized to play a critical role in learning and memory (Kerchner and Nicoll, 2008). Loss of these synapses would be expected to cause a fundamental disruption of hippocampal circuitry (Amaral and Lavenex, 2007; Insausti and Amaral, 2012). In fact, one postmortem electron microscopic study revealed a gradient of synaptic loss in CA1-SRLM from normal controls to MCI to mild AD, and that synaptic density correlated with memory performance (Scheff et al., 2007). It is thus likely that focal damage to CA1-SRLM plays a direct role in memory dysfunction in AD.

Other lines of evidence support the general notion that synaptic dysfunction is more pronounced than neuronal loss in early AD (Selkoe, 2002). In a mouse model of the disease, CA1 synaptic loss precedes both neuronal loss and the appearance of pathology (Hsia et al., 1999). In humans with early AD, pathological burden is greater in CA1-SRLM than in CA1-SP (Braak and Braak, 1997); supporting that finding, 7 T imaging revealed no difference in CA1-SP thickness between patients with mild AD and normal controls (Kerchner et al., 2010). In this study, delayed recall correlated significantly with both CA1-SRLM and CA1-SP thicknesses. Given our small sample size, it was not possible to detect whether one played a bigger role than the other in accounting for differences in episodic memory performance; this will be a focus of future work, which should involve the study of individuals at earlier, preclinical stages of Alzheimer's disease when discrepant contributions of CA1-SRLM and CA1-SP may be more pronounced.

In our patients, ERC thickness also correlated with both delayed free recall and delayed recognition subtests. This is not surprising, given the important reciprocal synaptic connections between CA1 and ERC (Amaral and Lavenex, 2007; Insausti and Amaral, 2012), and the early pathological involvement of the ERC in AD (Braak et al., 2006). Another group found that ERC thinning correlated with apolipoprotein-E ε4 allele carrier status, a risk factor for AD (Burggren et al., 2008), and with risk for subsequent memory decline among patients with MCI (Burggren et al., 2011). In this study, ERC width correlated significantly with CA1-SP width, emphasizing the important association of these loci.

Immediate recall did not appear to correlate significantly with any medial temporal metric. Although our small sample size makes it hard to be sure that no relationship exists, it is notable that immediate memory is thought to localize to non-hippocampal working memory pathways in the brain. Digit span is another metric of working memory, and its negative correlation with CA1-SRLM thickness (Table 2) is of uncertain significance; for immediate recall, the regression lines with the various medial temporal metrics, while not significant, all had a positive slope (Fig. 3), suggesting that there was no unifying pattern between these two methods of assessing working memory. Similarly, while there was a significant correlation between performance on one visuospatial task (figure copy) and the manually-derived CA1-SRLM data (Table 2), this finding was not reproduced on either of the other two visuospatial tasks (Block Design and Matrix Reasoning). Finally, DG/CA3 area correlated significantly with full scale IQ, a global metric of intelligence, but not with any measure of memory, any other specific cognitive domain, or the size of any other subfield. By contrast to these isolated findings, the relationship between hippocampal microstructure and delayed memory performance was consistent across tests and methods of measurement (Tables 2 and 3).

Do CA1-SRLM, CA1-SP, or ERC play specific roles in delayed recall? In theory, disruption of any node along the hippocampal trisynaptic loop (Amaral and Lavenex, 2007; Insausti and Amaral, 2012) could lead to medial temporal circuit dysfunction and memory failure. In this case, memory performance might be expected to degrade in direct proportion to the overall burden of pathology, wherever it first presents; in other words, the relationship between atrophy of these structures and memory performance that we observed may be nonspecific — reflecting only their particular vulnerability to early tau pathology but not any specific role in delayed recall capacity. Favoring instead a more specific role for CA1 is one lab's observation that among patients with temporal lobe epilepsy and mesial temporal sclerosis, a correlation between CA1 size and delayed recall performance emerged (Mueller et al., 2011b) just as it did in AD (Mueller et al., 2011a), despite somewhat different patterns of subfield atrophy in the two conditions (Mueller et al., 2009, 2010). It would be of interest to study other patients with different sorts of focal hippocampal lesions, in order to determine whether structural perturbations of different subfields or strata of the hippocampus lead to discrete neuropsychological outcomes. Given a special role of the hippocampus – and of the CA1 subfield in particular – for place memory (Bartsch et al., 2010), future work should incorporate navigational testing into the neuropsychological assessment.

Potential importance of the left hippocampus

Among our subjects, left and right hippocampal cross-sectional areas were equal, on average, and tightly correlated. Individual subfields – CA1-SRLM, CA1-SP, and DG/CA3 – were symmetric on average, but exhibited poor left-right correlation. While increased noise associated with the measurement of tiny structures could account for these poor correlations, these data suggest that macroscopic symmetries may belie actual smaller-scale asymmetries in the contributions of individual subfields and strata to overall hippocampal size.

This phenomenon relates to our finding that although left and right CA1-SRLM width was no different *on average*, the left side played a significantly greater role than the right in driving the relationship with delayed memory performance. There is substantial evidence that the left and right hippocampi contribute differentially to the encoding of verbal and visuospatial memory (Apostolova et al., 2010a; de Toledo-Morrell et al., 2000; Frisk and Milner, 1990; Milner, 1965; Nunn et al., 1998, 1999; Petrides and Milner, 1982; Smith and Milner, 1981; Spiers et al., 2001). Thus while it is reassuring to see a disproportionate role for the left CA1-SRLM (and ERC) in predicting performance on LM, a verbal contextual memory test, it is not clear why a similar trend was apparent for the visuospatial memory

test (Table 3). Perhaps this reflects a peculiarity of our subjects or of the BVMT-R; for instance, it is hard to control for the possibility that subjects may employ a verbal strategy to recall shapes and positions. Importantly, all of our subjects were right-handed, and so variations in hemispheric dominance should not be an issue. Other work suggests that the relationship between visuospatial memory and the right hippocampus is weaker than between verbal memory and the left (McDermid Vaz, 2004). Acquiring data on more AD subjects using additional visuospatial memory metrics could help to verify and expand upon this finding.

7 T hippocampal microstructural MRI: methodology

In addition to the findings outlined above, we demonstrate the utility of a high-resolution T2-weighted 7 T MRI sequence in reliably depicting hippocampal subfield and stratal microstructural anatomy. The sequence was well-tolerated among our elderly, mildly demented patients without any significant adverse effect.

One trade-off to having a high in-plane resolution (220 μm) was a low through-plane resolution (1.5 mm), which was necessary to maintain an adequate signal-to-noise ratio. Thick slices could produce partial volume artifacts, potentially blurring small structural features in-plane. We tried to compensate for this potential pitfall by carefully prescribing image acquisition perpendicular to the longitudinal axis of the hippocampus and by restricting our analysis to the hippocampal body, where the anatomy is much more dynamic in-plane than through-plane. Future sequence development could focus on strategies to reduce slice thickness, which may allow more detailed analysis of the hippocampal head, where anatomy is dynamic in all three dimensions.

We also report a semi-automated method for hippocampal stratal width determination. This technique reduces reliance on user intervention to measure small structures, with the hope of speeding analysis and enhancing reproducibility. We found that the method yielded estimates of CA1-SRLM and CA1-SP width that correlated well with manual measurements. Manual and semi-automated measurements correlated at a high level of significance but were not perfectly linked, and it is not necessarily straightforward to predict which method should be more accurate. While manual measurements are typically considered to be a gold standard, the semi-automated method, which integrates many measurements along the full length of the region of interest (compared to three manual measurements per slice), could possibly be less susceptible to noise. The semi-automated tool does still require the input of a user who is knowledgeable of hippocampal anatomy and so is not widely deployable, but it sets the stage for future development of a more fully automated analysis.

Conclusions

In sum, we found that among patients with mild AD, delayed recall performance correlates with CA1-SRLM, CA1-SP, and ERC widths. Left CA1-SRLM width played an especially important role in predicting delayed recall capacity. These data suggest that in addition to being a marker for the presence of AD pathology, CA1-SRLM atrophy closely tracks the magnitude of episodic memory impairment among patients with the disease. While it is not yet clear whether a high-resolution imaging biomarker of AD-associated memory loss is yet poised to assist in the early diagnosis of AD, our findings suggest that it may be useful in tracking disease severity. In future work, it will be important to follow patients longitudinally, and to examine patients with MCI or normal cognition at baseline.

Acknowledgments

We thank Christina Wyss-Coray, RN, Jeffrey Bernstein, BA, and Jennie Lambert-Lynch, BA, for patient recruitment and study logistics, as well as Mohammad-Mehdi Khalighi, PhD for work on 7 T MRI sequence development. This work was supported by grants from the Alzheimer's Association to GAK (NIRG-11-205493) and from the NIH to BKR (P41 RR09784).

References

Amaral, D.; Lavenex, P. Hippocampal neuroanatomy. In: Andersen, P.; Morris, R.; Amaral, D.; Bliss, T.; O'Keefe, J., editors. The Hippocampus Book. New York: Oxford University Press; 2007. p. 37-114.

Apostolova LG, Dinov ID, Dutton RA, Hayashi KM, Toga AW, Cummings JL, Thompson PM. 3D comparison of hippocampal atrophy in amnestic mild cognitive impairment and Alzheimer's disease. Brain. 2006a; 129:2867–2873. [PubMed: 17018552]

Apostolova LG, Dutton RA, Dinov ID, Hayashi KM, Toga AW, Cummings JL, Thompson PM. Conversion of mild cognitive impairment to Alzheimer disease predicted by hippocampal atrophy maps. Arch. Neurol. 2006b; 63:693–699. [PubMed: 16682538]

Apostolova LG, Morra JH, Green AE, Hwang KS, Avedissian C, Woo E, Cummings JL, Toga AW, Jack CR Jr, Weiner MW, Thompson PM. Automated 3D mapping of baseline and 12-month associations between three verbal memory measures and hippocampal atrophy in 490 ADNI subjects. NeuroImage. 2010a; 51:488–499. [PubMed: 20083211]

Apostolova LG, Mosconi L, Thompson PM, Green AE, Hwang KS, Ramirez A, Mistur R, Tsui WH, de Leon MJ. Subregional hippocampal atrophy predicts Alzheimer's dementia in the cognitively normal. Neurobiol. Aging. 2010b; 31:1077–1088. [PubMed: 18814937]

Atienza M, Atalaia-Silva KC, Gonzalez-Escamilla G, Gil-Neciga E, Suarez-Gonzalez A, Cantero JL. Associative memory deficits in mild cognitive impairment: the role of hippocampal formation. NeuroImage. 2011; 57:1331–1342. [PubMed: 21640840]

Bartsch T, Schonfeld R, Muller FJ, Alfke K, Leplow B, Aldenhoff J, Deuschl G, Koch JM. Focal lesions of human hippocampal CA1 neurons in transient global amnesia impair place memory. Science. 2010; 328:1412–1415. [PubMed: 20538952]

Benedict, R. Brief Visuospatial Memory Test-Revised. Odessa, FL: Psychological Assessment Resources, Inc; 1997.

Braak E, Braak H. Alzheimer's disease: transiently developing dendritic changes in pyramidal cells of sector CA1 of the Ammon's horn. Acta Neuropathol. 1997; 93:323–325. [PubMed: 9113196]

Braak H, Alafuzoff I, Arzberger T, Kretzschmar H, Del Tredici K. Staging of Alzheimer disease-associated neurofibrillary pathology using paraffin sections and immunocytochemistry. Acta Neuropathol. 2006; 112:389–404. [PubMed: 16906426]

Brandt J. The Hopkins verbal learning test: development of a new memory test with six equivalent forms. Clin. Neuropsychol. 1991; 5:125–142.

Burggren AC, Zeineh MM, Ekstrom AD, Braskie MN, Thompson PM, Small GW, Bookheimer SY. Reduced cortical thickness in hippocampal subregions among cognitively normal apolipoprotein E e4 carriers. NeuroImage. 2008; 41:1177–1183. [PubMed: 18486492]

Burggren AC, Renner B, Jones M, Donix M, Suthana NA, Martin-Harris L, Ercoli LM, Miller KJ, Siddarth P, Small GW, Bookheimer SY. Thickness in entorhinal and subicular cortex predicts episodic memory decline in mild cognitive impairment. IntJAlzheimer's Dis. 2011; 2011:956053.

Cummings JL, Mega M, Gray K, Rosenberg-Thompson S, Carusi DA, Gornbein J. The neuropsychiatric inventory: comprehensive assessment of psychopathology in dementia. Neurology. 1994; 44:2308–2314. [PubMed: 7991117]

de Toledo-Morrell L, Dickerson B, Sullivan MP, Spanovic C, Wilson R, Bennett DA. Hemispheric differences in hippocampal volume predict verbal and spatial memory performance in patients with Alzheimer's disease. Hippocampus. 2000; 10:136–142. [PubMed: 10791835]

Eldridge LL, Engel SA, Zeineh MM, Bookheimer SY, Knowlton BJ. A dissociation of encoding and retrieval processes in the human hippocampus. J. Neurosci. 2005; 25:3280–3286. [PubMed: 15800182]

Frisk V, Milner B. The role of the left hippocampal region in the acquisition and retention of story content. Neuropsychologia. 1990; 28:349–359. [PubMed: 2111523]

Gladsjo JA, Schuman CC, Evans JD, Peavy GM, Miller SW, Heaton RK. Norms for letter and category fluency: demographic corrections for age, education, and ethnicity. Assessment. 1999; 6:147–178. [PubMed: 10335019]

Hsia AY, Masliah E, McConlogue L, Yu GQ, Tatsuno G, Hu K, Kholodenko D, Malenka RC, Nicoll RA, Mucke L. Plaque-independent disruption of neural circuits in Alzheimer's disease mouse models. Proc. Natl. Acad. Sci. U. S. A. 1999; 96:3228–3233. [PubMed: 10077666]

Insausti, R.; Amaral, DG. Hippocampal formation. In: Mai, JK.; Paxinos, G., editors. Atlas of the Human Brain. Third Edition. London: Elsevier Academic Press; 2012. p. 896-942.

Kerchner GA. Ultra-high field 7 T MRI: a new tool for studying Alzheimer's disease. J. Alzheimers Dis. 2011; 22(Suppl. 3):91–95. [PubMed: 21971453]

Kerchner GA, Nicoll RA. Silent synapses and the emergence of a postsynaptic mechanism for LTP. Nat. Rev. Neurosci. 2008; 9:813–825. [PubMed: 18854855]

Kerchner GA, Hess CP, Hammond-Rosenbluth KE, Xu D, Rabinovici GD, Kelley DAC, Vigneron DB, Nelson SJ, Miller BL. Hippocampal CA1 apical neuropil atrophy in mild Alzheimer disease visualized with 7-T MRI. Neurology. 2010; 75:1381–1387. [PubMed: 20938031]

La Joie R, Fouquet M, Mézenge F, Landeau B, Villain N, Mevel K, Pélerin A, Eustache F, Desgranges B, Chételat G. Differential effect of age on hippocampal subfields assessed using a new high-resolution 3 T MR sequence. NeuroImage. 2010; 53:506–514. [PubMed: 20600996]

McDermid Vaz SA. Nonverbal memory functioning following right anterior temporal lobectomy: a meta-analytic review. Seizure. 2004; 13:446–452. [PubMed: 15324819]

McKhann G, Drachman D, Folstein M, Katzman R, Price D, Stadlan EM. Clinical diagnosis of Alzheimer's disease: report of the NINCDS–ADRDA Work Group under the auspices of Department of Health and Human Services Task Force on Alzheimer's disease. Neurology. 2011; 77:333.

Meng X-L, Rosenthal R, Rubin DB. Comparing correlated correlation coefficients. Psychol. Bull. 1992; 111:172–175.

Milner B. Visually-guided maze learning in man: effects of bilateral hippocampal, bilateral frontal, and unilateral cerebral lesions. Neuropsychologia. 1965; 3:317–338.

Milner B. The medial temporal-lobe amnesic syndrome. Psychiatr. Clin. North Am. 2005; 28:599–611. [PubMed: 16122569]

Mizutani T, Kasahara M. Hippocampal atrophy secondary to entorhinal cortical degeneration in Alzheimer-type dementia. Neurosci. Lett. 1997; 222:119–122. [PubMed: 9111743]

Morris JC. The clinical dementia rating (CDR): current version and scoring rules. Neurology. 1993; 43:2412–2414. [PubMed: 8232972]

Mueller SG, Stables L, Du AT, Schuff N, Truran D, Cashdollar N, Weiner MW. Measurement of hippocampal subfields and age-related changes with high resolution MRI at 4 T. Neurobiol. Aging. 2007; 28:719–726. [PubMed: 16713659]

Mueller SG, Laxer KD, Barakos J, Cheong I, Garcia P, Weiner MW. Subfield atrophy pattern in temporal lobe epilepsy with and without mesial sclerosis detected by high-resolution MRI at 4 Tesla: preliminary results. Epilepsia. 2009; 50:1474–1483. [PubMed: 19400880]

Mueller SG, Schuff N, Yaffe K, Madison C, Miller B, Weiner MW. Hippocampal atrophy patterns in mild cognitive impairment and Alzheimer's disease. Hum. Brain Mapp. 2010; 31:1339–1347. [PubMed: 20839293]

Mueller SG, Chao LL, Berman B, Weiner MW. Evidence for functional specialization of hippocampal subfields detected by MR subfield volumetry on high resolution images at 4 T. NeuroImage. 2011a; 56:851–857. [PubMed: 21419225]

Mueller SG, Laxer KD, Scanlon C, Garcia P, McMullen WJ, Loring DW, Meador KJ, Weiner MW. Different structural correlates for verbal memory impairment in temporal lobe epilepsy with and without mesial temporal lobe sclerosis. Hum. Brain Mapp. 2011b; 33:489–499. [PubMed: 21438080]

Nunn JA, Polkey CE, Morris RG. Selective spatial memory impairment after right unilateral temporal lobectomy. Neuropsychologia. 1998; 36:837–848. [PubMed: 9740357]

Nunn JA, Graydon FJX, Polkey CE, Morris RG. Differential spatial memory impairment after right temporal lobectomy demonstrated using temporal titration. Brain. 1999; 122:47–59. [PubMed: 10050894]

Petrides M, Milner B. Deficits on subject-ordered tasks after frontal- and temporal-lobe lesions in man. Neuropsychologia. 1982; 20:249–262. [PubMed: 7121793]

Pfeffer RI, Kurosaki TT, Harrah CH Jr, Chance JM, Filos S. Measurement of functional activities in older adults in the community. J. Gerontol. 1982; 37:323–329. [PubMed: 7069156]

Prudent V, Kumar A, Liu S, Wiggins G, Malaspina D, Gonen O. Human hippocampal subfields in young adults at 7.0 T: feasibility of imaging. Radiology. 2010; 254:900–906. [PubMed: 20123900]

Qin S, Hu X-Y, Xu H, Zhou J-N. Regional alteration of synapsin I in the hippocampal formation of Alzheimer's disease patients. Acta Neuropathol. 2004; 107:209–215. [PubMed: 14673601]

Randolph C, Tierney MC, Mohr E, Chase TN. The repeatable battery for the assessment of neuropsychological status (RBANS): preliminary clinical validity. J. Clin. Exp. Neuropsychol. 1998; 20:310–319. [PubMed: 9845158]

Rosset A, Spadola L, Ratib O. OsiriX: an open-source software for navigating in multidimensional DICOM images. J. Digit. Imaging. 2004; 17:205–216. [PubMed: 15534753]

Scheff SW, Price DA, Schmitt FA, DeKosky ST, Mufson EJ. Synaptic alterations in CA1 in mild Alzheimer disease and mild cognitive impairment. Neurology. 2007; 68:1501–1508. [PubMed: 17470753]

Selkoe DJ. Alzheimer's disease is a synaptic failure. Science. 2002; 298:789–791. [PubMed: 12399581]

Smith ML, Milner B. The role of the right hippocampus in the recall of spatial location. Neuropsychologia. 1981; 19:781–793. [PubMed: 7329524]

Spiers HJ, Burgess N, Maguire EA, Baxendale SA, Hartley T, Thompson PJ, O'Keefe J. Unilateral temporal lobectomy patients show lateralized topographical and episodic memory deficits in a virtual town. Brain. 2001; 124:2476–2489. [PubMed: 11701601]

Thal DR, Holzer M, Rub U, Waldmann G, Gunzel S, Zedlick D, Schober R. Alzheimer-related tau-pathology in the perforant path target zone and in the hippocampal stratum oriens and radiatum correlates with onset and degree of dementia. Exp. Neurol. 2000; 163:98–110. [PubMed: 10785448]

Wechsler, D. Wechsler Memory Scale. 3 ed. San Antonio: The Psychological Corporation; 1997.

Wechsler, D. Wechsler Abbreviated Scale of Intelligence. New York, NY: The Psychological Corporation: Harcourt Brace & Company; 1999.

Yassa MA, Stark SM, Bakker A, Albert MS, Gallagher M, Stark CEL. High-resolution structural and functional MRI of hippocampal CA3 and dentate gyrus in patients with amnestic mild cognitive impairment. NeuroImage. 2010; 51:1242–1252. [PubMed: 20338246]

Yesavage JA. Geriatric depression scale. Psychopharmacol. Bull. 1988; 24:709–711. [PubMed: 3249773]

Yushkevich PA, Avants BB, Pluta J, Das S, Minkoff D, Mechanic-Hamilton D, Glynn S, Pickup S, Liu W, Gee JC, Grossman M, Detre JA. A high-resolution computational atlas of the human hippocampus from postmortem magnetic resonance imaging at 9.4 T. NeuroImage. 2009; 44:385–398. [PubMed: 18840532]

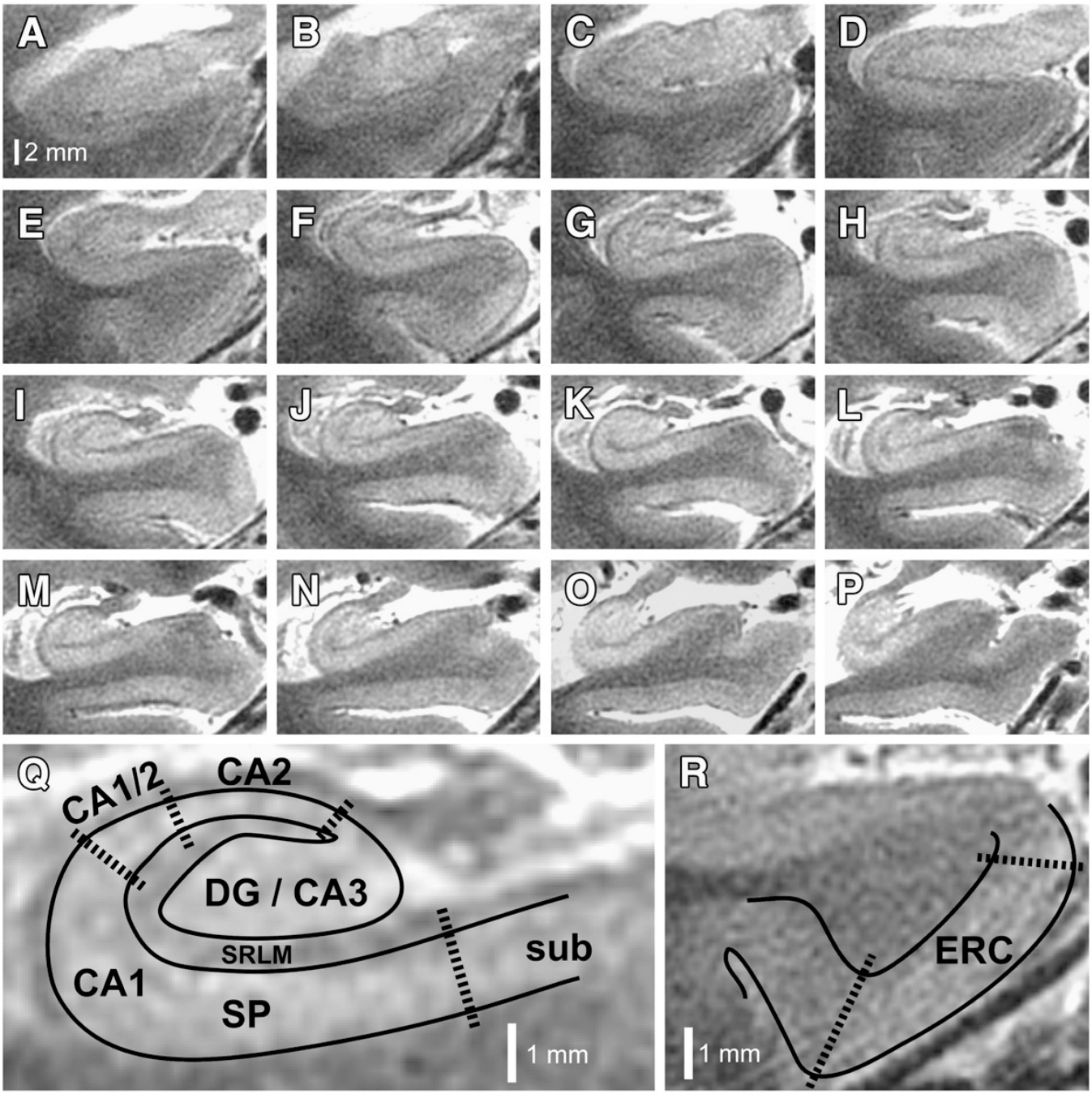

Fig. 1.

7 T hippocampal microstructural imaging. (A–P) Serial oblique coronal slices, zoomed to the right hippocampus, are illustrated for one of the patients enrolled in this study. Slices are arranged anterior to posterior, using the same scale represented by the bar in panel (A). (Q) Higher magnification view of panel (I), illustrating how subfields are demarcated. Areas containing dense collections of neuronal cell bodies (e.g., CA1-SP) appear bright on this T2-weighted image, whereas neuropil areas (e.g., CA1-SRLM), which contain dense tangles of axons, dendrites, and synapses, appear relatively hypointense. DG, dentate gyrus; CA1–3, cornus ammonis subfields 1–3; SP, stratum pyramidale; SRLM, stratum radiatum/stratum

lacunosum-moleculare; sub, subiculum. (R) Higher magnification of the parahippocampal gyrus from panel (E), illustrating how the entorhinal cortex (ERC) is demarcated.

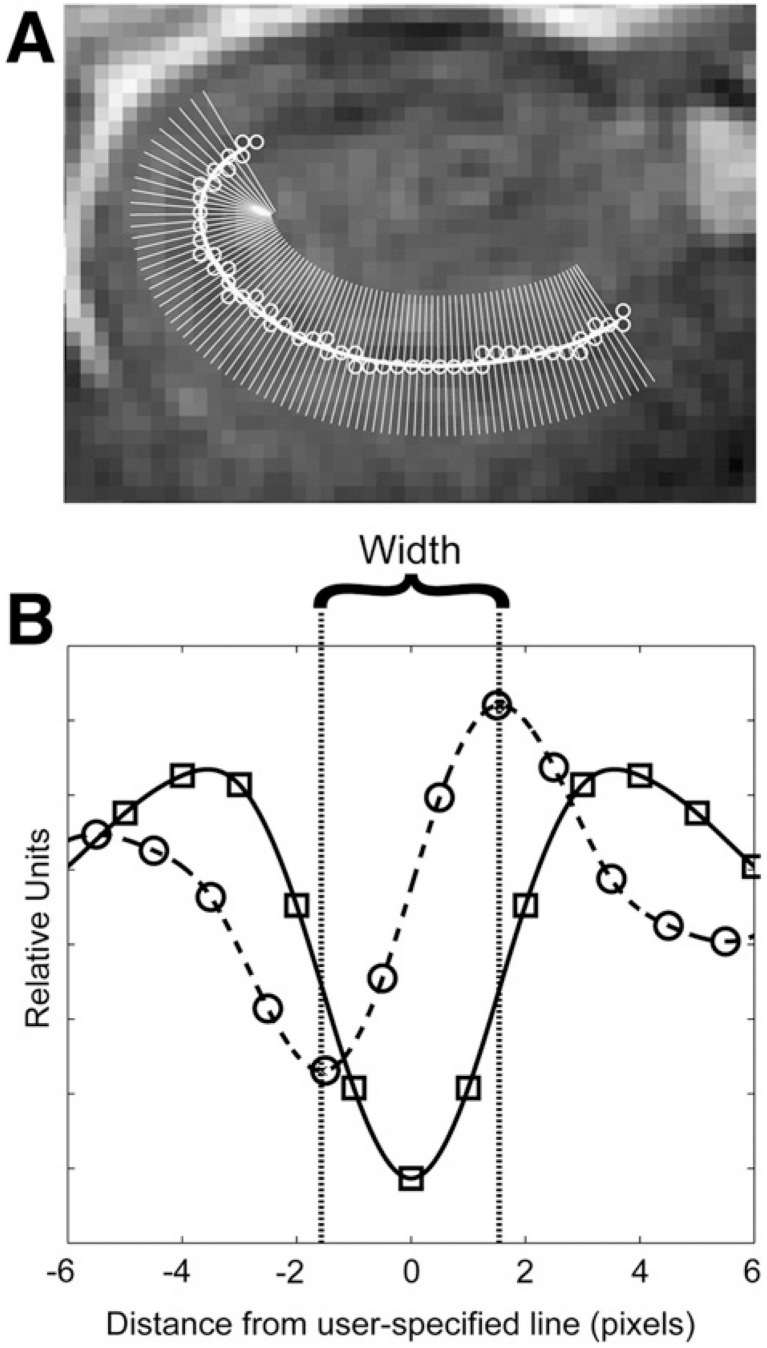

Fig. 2.

Semi-automated stratal width determination. (A) Superimposed on an image of the right hippocampus in one patient is a user-specified line through the CA1-SRLM (open circles). The thick white line is the spline fit to the user-specified line, and thin white lines delineate the direction of the orthogonal vectors derived from the algorithm described in Methods. (B) Average T2 signal intensity (in relative units) is plotted against distance from the user-specified line (in pixels). Squares represent measured values, and the solid line is a spline fit through those points, as described in Methods. The dashed line and circles correspond to the first derivative. The width of the stratum of interest is defined as the distance between the peak and the trough of this first derivative.

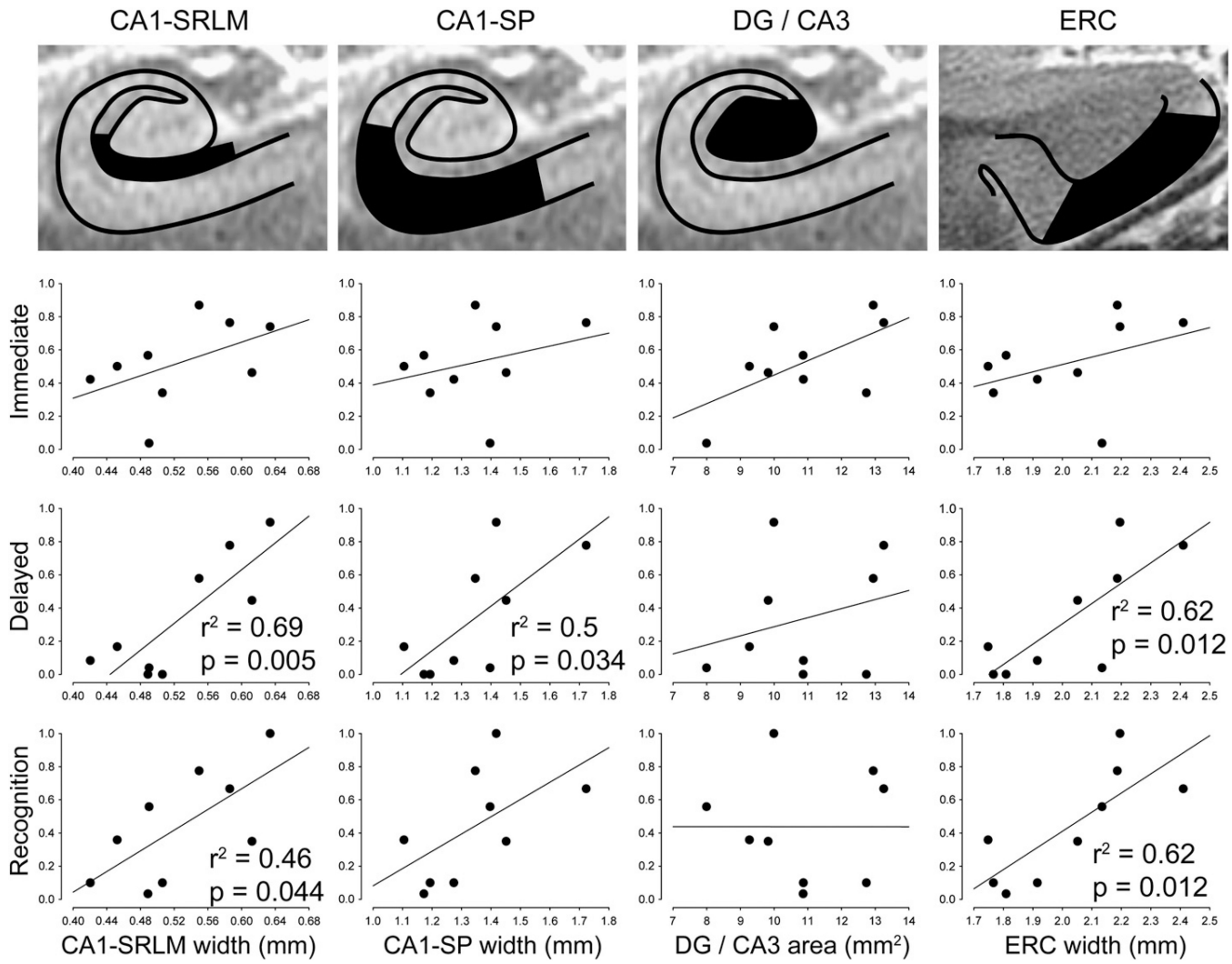

Fig. 3.

Microstructural correlates of memory performance. Scatter plots are illustrated for composite scores of immediate recall, delayed recall, and delayed recognition (see Methods), versus each of the main microstructural metrics: CA1-SRLM width, CA1-SP width, DG/CA3 cross-sectional area, and ERC width. Statistics are shown only for significant correlations; also see Table 2. CA1-SRLM and CA1-SP widths were determined using a semi-automated method (see Fig. 2).

Table 1

Subjects.

Number	**9**
Demographics	
Age (range)	68 ± 9 (57–85)
M:F	4:5
Education (years)	16 ± 3
Functional measures	
MMSE	24.7 ± 2.7
CDR (range)	0.5–1.0
CDR-SB	4.4 ± 1.3
FAQ	15.3 ± 6.2
Memory performance	
HVLT-R immediate recall (raw score, out of 36)	13 ± 2.8
HVLT-R delayed recall (raw score, out of 12)	1.6 ± 2.1
HVLT-R delayed recognition (hits minus false positives)	4.3 ± 3.6
BVMT-R immediate recall (raw score, out of 36)	6.7 ± 6.1
BVMT-R delayed recall (raw score, out of 12)	1.7 ± 1.7
BVMT-R delayed recognition (hits minus false positives)	3.8 ± 2.7
LM 1 (scaled score)	5 ± 2.4
LM 2 (scaled score)	4.1 ± 3.6
LM percent retention (scaled score)	7.3 ± 4.6
Other psychometric measures	
Full scale IQ	92 ± 15
Digit span (scaled score)	7.7 ± 1.7
Category Fluency (T-score)	32 ± 6.2
Trails B (T-score)	15 ± 20
Boston Naming Test (T-score)	40 ± 11
Figure copy (T-score)	30 ± 22
Block Design (T-Score)	40 ± 11
Matrix Reasoning (T-score)	46 ± 14

BVMT-R, Brief Visuospatial Memory Test, Revised;
CDR, Clinical Dementia Rating Score;
CDR-SB, CDR sum of boxes score;
FAQ, Functional Activities Questionnaire;
HVLT-R, Hopkins Verbal Learning Test, Revised;
LM, Logical Memory subtest of the Wechsler Memory Scale, 3rd edition.
MMSE, Mini Mental State Examination;

Table 2

Medial temporal microstructural metrics in relation to each other and to clinical metrics.

	CA1-SRLM		CA1-SP		DG/CA3	ERC	Hipp
	Aut	Man	Aut	Man			
Demographics							
Age	0.02	0.01	0.02	0.02	0.37^	0	0.01
Education	0.11	0.01	0	0.02	0.15	0.01	0.01
Gender	n.s.†	n.s.	n.s.	n.s.	n.s.	n.s.	n.s.
Subfields							
CA1-SRLM	–		–		–	–	–
CA1-SP	0.44^	0.22	–		–	–	–
DG/CA3	0.03	0.05	0.06	0.17	–	–	–
ERC	0.44^	0.28	0.87**	0.73**	0.05	–	–
Hipp	0.55*	0.23	0.68**	0.90**	0.38^	0.59*	–
Memory							
Immediate recall	0.24	0.05	0.08	0.22	0.38^	0.16	0.36^
Delayed recall	0.69**	0.51*	0.50*	0.57*	0.08	0.62*	0.61*
Delayed recognition	0.46*	0.45*	0.33	0.42^	0	0.62*	0.33
Other psychometrics							
Full scale IQ	0	0.13	0	0	0.54*	0.02	0.05
Digit span	0.35†† ,^	0.65†† ,**	0.22	0.16	0.07	0.13	0.14
Category Fluency	0.01	0.01	0	0	0.01	0.04	0.01
Trails B	0.35^	0.43^	0.11	0.28	0.05	0.09	0.21
Boston Naming Test	0.30	0.17	0.15	0.01	0	0.02	0.03
Figure copy	0.23	0.47*	0.27	0.07	0.22	0.19	0.03
Block Design	0.08	0.19	0.06	0.16	0.10	0.03	0.07
Matrix Reasoning	0.06	0.29	0	0	0.43^	0.01	0.01

For each category (except for gender, see below), the fraction of variance shared with each hippocampal subfield metric is illustrated (Pearson r^2). All trends and significant correlations were direct (positive Pearson coefficient), except as indicated (††). For CA1-SRLM and CA1-SP, correlation coefficients are shown for data derived from the semi-automated (Aut) and manual (Man) techniques (see Methods).

^ Non-significant trend, with $p<0.10$.

† T-tests were performed to look for gender differences; for each comparison, the difference in means was not significant (n.s.).

CA1–3, cornus ammonis subfields 1–3; DG, dentate gyrus; SP, stratum pyramidale; SRLM, stratum radiatum/stratum lacunosum-moleculare; ERC, entorhinal cortex; Hipp, hippocampus.

* $p<0.05$.

** $p<0.01$.

Table 3

Lateralized relationships between medial temporal structural metrics and individual memory subtests.

	CA1-SRLM		CA1-SP		ERC	
	Left	**Right**	**Left**	**Right**	**Left**	**Right**
Hopkins Verbal Learning Test-Revised						
Immediate	0.02	0.16	0.2	0.01	0.01	0.03
Delayed	0.72 **	0.45 *	0.09	0.26	0.38 ^	0.20
Recognition	0.52 *	0.05	0.13	0.27	0.49 *	0.41 ^
Wechsler Memory Scale-III/Logical Memory Test						
Immediate	0.45 *	0.11	0.17	0.28	0.15	0.17
Delayed	0.94 **,††	0.23	0.30	0.70 **	0.60 *	0.41 ^
Recognition	0.57 *	0.14	0.10	0.54 *	0.81 **,†	0.21
Brief Visuospatial Memory Test-Revised						
Immediate	0.26	0	0.13	0.14	0.41 ^	0.34 ^
Delayed	0.46 *	0.01	0.13	0.29	0.40 ^	0.38 ^
Recognition	0.54 *	0.15	0.02	0.37 ^	0.50 *	0.19

For each category, the fraction of variance shared with each imaging metric is illustrated (Pearson r^2). All trends and significant correlations were direct (positive Pearson coefficient). For CA1-SRLM and CA1-SP, correlation coefficients are shown for data derived from the semi-automated technique (see Fig. 2).

^ Non-significant trend, with $p<0.10$.

†,†† Significantly different from the contralateral correlation coefficient by Steiger's Z statistic (†: $p<0.05$; ††: $p<0.01$); see Section Statistics (Meng et al., 1992).

CA1–3, cornus ammonis subfields 1–3; SP, stratum pyramidale; SRLM, stratum radiatum/stratum lacunosum-moleculare; ERC, entorhinal cortex.

* $p<0.05$.

** $p<0.01$.